Phase-field model of insulator-to-metal transition in VO_2 under an electric field

Yin Shi* and Long-Qing Chen†

Department of Materials Sciences and Engineering, Pennsylvania State University, University Park, Pennsylvania 16802, USA

(Received 22 February 2018; revised manuscript received 9 May 2018; published 23 May 2018)

The roles of an electric field and electronic doping in insulator-to-metal transitions are still not well understood. Here we formulated a phase-field model of insulator-to-metal transitions by taking into account both structural and electronic instabilities as well as free electrons and holes in VO_2, a strongly correlated transition-metal oxide. Our phase-field simulations demonstrate that in a VO_2 slab under a uniform electric field, an abrupt universal resistive transition occurs inside the supercooling region, in sharp contrast to the conventional Landau-Zener smooth electric breakdown. We also show that hole doping may decouple the structural and electronic phase transitions in VO_2, leading to a metastable metallic monoclinic phase which could be stabilized through a geometrical confinement and the size effect. This work provides a general mesoscale thermodynamic framework for understanding the influences of electric field, electronic doping, and stress and strain on insulator-to-metal transitions and the corresponding mesoscale domain structure evolution in VO_2 and related strongly correlated systems.

DOI: 10.1103/PhysRevMaterials.2.053803

I. INTRODUCTION

Vanadium dioxide (VO_2), a strongly correlated transition-metal oxide, undergoes a first-order insulator-to-metal transition (IMT) from a monoclinic insulator (M1) to a rutile metal (R) at $T_c = 338$ K upon heating [1]. The coexistence of the strong electron correlation and the V dimerization obscures the nature of the resistive transition in VO_2. While the strong dimerization suggests a Peierls transition, recent microscopic theories uncovered the crucial role of the electron correlation [2–4]. Moreover, recent experiments demonstrated that the structural and electronic phase transitions in VO_2 may be decoupled, e.g., through a contact of a VO_2 nanobeam with a metallic substrate [5], an elastic constraint on a VO_2 thin film [6], or a combination of hole doping and geometrical confinement for a VO_2 thin film [7]. Therefore, it is imperative that both structural and electronic instabilities are incorporated in any thermodynamic theory of the IMT in VO_2.

A sufficient amount of free charges may alter the IMT by screening the electron-electron repulsion and thus reducing the electron correlation [8]. It was experimentally demonstrated that an applied electric field is able to drive the IMT via a field-induced charge accumulation. In a VO_2 transistor, the bulk conductive channels open up collectively above a threshold voltage, with an extension far exceeding the Thomas-Fermi screening length [9]. This is in sharp contrast to the standard field-induced Landau-Zener breakdown activated smoothly at a field of the order of the energy gap, which is predicted by the across-gap tunneling [10,11]. There is also experimental evidence that demonstrates the ability of electronic doping, i.e., introduction of holes or electrons through solute dopants and defects, to modulate the IMT in VO_2, e.g., in doped $M_xV_{1-x}O_2$ ($M = Ti^{4+}$, W^{6+}, Mo^{6+}, or Nb^{5+}) [12] and VO_2-$VO_{2-\delta}$ bilayers [7]. The measurement of the phase transitions in the VO_2-$VO_{2-\delta}$ bilayer further unveiled the presence of a metallic monoclinic (MM) phase in the hole-doped and geometrically confined VO_2 layer [7]. Such a MM phase is, however, absent in the pristine bulk VO_2.

Although the microscopic quantum theories may provide physical insights into the IMT at the electronic structure level [2–4], the mesoscale mechanisms and domain evolution during the IMT of a doped crystal under an electric field and/or stress require mesoscale continuum models that take into account the electron correlation, structural changes, and the presence of free charges. In this article, we formulate a phase-field model with the thermodynamics described by a Landau potential as a function of structural order parameters, spin-correlation order parameters [13], and free electron and hole concentrations. As an example, we study the electric breakdown of a VO_2 slab under a uniform electric field. It is shown that inside the supercooling region, it occurs through an abrupt universal IMT, in sharp contrast to the smooth Landau-Zener breakdown. We then study the IMT in a VO_2-$VO_{2-\delta}$ bilayer and show that hole doping in the VO_2 layer may induce a metastable MM phase which could be stabilized via a geometrical confinement between the two layers and the size effect.

II. THERMODYNAMICS OF A LATTICE-ELECTRON SYSTEM

By examining the symmetry breaking of the magnetic group during the IMT, we previously formulated a bulk Landau potential incorporating a set of structural order parameters $\eta_i, i = 1,2,3,4$ and a set of spin-correlation order parameters $\mu_i, i = 1,2,3,4$ (characterizing the magnetic order) to explicitly describe the structural and electronic transitions during the

*yxs187@psu.edu
†lqc3@psu.edu

IMT in the *pristine* VO_2 [13]. It reads (per unit cell) [13]

$$F(\eta,\mu) = \frac{a}{2}\frac{T-T_0}{T_c}\eta_i\eta_i + \frac{b_{ij}}{4}\eta_i^2\eta_j^2 + \frac{c_{ij}}{6}\eta_i^2\eta_j^4 + \frac{A}{2}\frac{T-T_0'}{T_c}\mu_i\mu_i + \frac{B_{ij}}{4}\mu_i^2\mu_j^2 + \frac{C_{ij}}{6}\mu_i^2\mu_j^6 + g\eta_i\mu_i - \frac{g_{ijkl}}{2}\eta_i\eta_j\mu_k\mu_l + \frac{q_{ijkl}}{2}\eta_i\eta_j\eta_k\mu_l, \quad (1)$$

where T is the temperature and other parameters are constants (satisfying certain symmetry relations [13]), and the Einstein summation convention is used. A finite η_i indicates the dimerization of the neighboring V atoms, and a finite μ_i indicates the formation of the dynamical singlet situated on the neighboring V sites [13], which may be directly related to the opening of the energy gap [2–4]. Hereafter, we simplify the description of the theory by reducing the four-dimensional order parameters η_i and μ_i to one-dimensional order parameters $\eta \equiv \sqrt{\sum_i \eta_i^2}$ and $\mu \equiv -\sqrt{\sum_i \mu_i^2}$. The order parameter values for R, M1, and MM phases are $(\eta = 0, \mu = 0)$, $(\eta \neq 0, \mu \neq 0)$, and $(\eta \neq 0, \mu = 0)$, respectively [13]. In the presence of free electrons and holes, the total bulk Landau potential can be written as a sum of the contribution from the pristine VO_2 and that from the free charges

$$\Omega_t(\eta,\mu,n,p) = F(\eta,\mu) + \Omega(\mu,n,p), \quad (2)$$

where n and p are the concentrations of the free electrons and holes, respectively. Ω is the (nonequilibrium) thermodynamic potential of the free charges. It must depend on the electronic order parameter μ. The equilibrium state can be determined by minimizing Ω_t with respect to all the order parameters η, μ, n, and p [14].

Ω may be approximated using the effective two-band model for semiconductors, in which the energy bands are approximated as only one band below (valence band, at energy E_v with an effective density of states N_v) and one band above (conduction band, at energy E_c with an effective density of states N_c) the Fermi level E_{F0} [15]. The equilibrium electron and hole concentrations at zero field can be approximated by the Boltzmann distribution, $n = N_c \exp[-(E_c - E_{F0})/k_BT]$ and $p = N_v \exp[-(E_{F0} - E_v)/k_BT]$ [15], where k_B is the Boltzmann constant. Substituting $E_{F0} = E_F + (E_c + E_v)/2$ into these expressions where E_F is the Fermi level measured from the midpoint of the energy gap, one can see that equivalently $n = N_c \exp[-(E_g/2 - E_F)/k_BT]$ and $p = N_v \exp[-(E_g/2 + E_F)/k_BT]$, where $E_g = E_c - E_v$ is the gap. Hence, referencing the midpoint of the gap, the energies of the electrons and holes are both $E_g/2$, while their chemical potentials are E_F and $-E_F$, respectively. Ω may then read (per unit cell)

$$\Omega = \frac{E_g}{2}(n+p) + eV(p-n) - TS - E_F(n - p + N_a - N_d) - \Omega_0. \quad (3)$$

Here V is the electric potential, e is the elementary charge, $S = -k_Bn[\ln(n/N_c) - 1] - k_Bp[\ln(p/N_v) - 1]$ is the entropy, and N_a and N_d are the acceptor and donor concentrations, respectively. $\Omega_0 = -2k_BTn_i$ is a reference energy with $n_i = \sqrt{N_cN_v}\exp(-E_g/2k_BT)$ being the intrinsic carrier concentration. Note that in the E_F term in Eq. (3), $(N_d - N_a)$ is subtracted from $(n - p)$; i.e., $(N_d - N_a)$ free charges, which are released from dopants, do not participate in the (nonequilibrium) process of particle number variation (recombination). This is because these dopants are assumed *a priori* to remain ionized. E_g can be approximated as [13]

$$E_g \approx \frac{2U^2\mu_0^2\mu^2}{k_BT_c}, \quad (4)$$

where U is the onsite Coulomb repulsion and μ_0 is a dimensionless parameter. Fitting this to the measured value of the energy gap ~0.67 eV of the M1 phase [16] with $U \sim 4$ eV [2], we obtain $\mu_0 = -0.025$. The minimization of Ω_t with respect to n and p gives $n = N_c \exp[-(E_g/2 - E_F - eV)/k_BT]$ and $p = N_v \exp[-(E_g/2 + E_F + eV)/k_BT]$, reconciling the Debye-Hückel approximation [17]. With the charge neutrality condition at zero field $n + N_a = p + N_d$, one also finds $E_F = k_BT \ln[\sqrt{\frac{N_v}{N_c}}\frac{(N_d-N_a)/2+\sqrt{(N_d-N_a)^2/4+n_i^2}}{n_i}]$. We note that mathematically E_F in Eq. (3) is a Lagrange multiplier for maintaining charge neutrality.

The Ω added to F in Eq. (2) may alter the IMT of the pristine VO_2. To see this, one can substitute n and p with their equilibrium values and leave Ω_t as a function of μ and η only, which allows for a convenient comparison between the total Landau potentials before and after the inclusion of Ω. In the zero field and intrinsic (no doping) case, one obtains $\Omega = 0$ and $\Omega_t(\eta,\mu) = F(\eta,\mu)$ at equilibrium, which recovers the Landau potential of the pristine VO_2. In the intrinsic case but with an applied electric field, one has $\Omega_t(\eta,\mu) = F(\eta,\mu) - 2k_BTn_i[\cosh(eV/k_BT) - 1]$ at equilibrium, which, by expansion to the first order of E_g (considering temperatures near T_c), gives

$$\Omega_t(\eta,\mu) \approx F(\eta,\mu) + [\cosh(eV/k_BT_c) - 1]\sqrt{N_cN_v}E_g, \quad (5)$$

in which the constant terms independent of η and μ have been dropped. Using Eq. (4), one finds that the E_g term added to F will renormalize the Curie-Weiss temperature of the spin-correlation order parameter, i.e., T_0' in Eq. (1), by always lowering it by an amount $4[\cosh(eV/k_BT_c) - 1]\sqrt{N_cN_v}U^2\mu_0^2/k_BA$. This indicates that the applied electric potential assists the transition from an insulator to a metal. In the doped case but at zero field, imagining hole doping $N_a \gg n_i$ and $N_d = 0$, one obtains at equilibrium $p \approx N_a \gg n \approx n_i^2/N_a$ and

$$\Omega_t(\eta,\mu) \approx F(\eta,\mu) + \frac{N_aE_g}{2}, \quad (6)$$

in which the constant terms independent of η and μ have also been dropped. Similar to the case with the applied electric field, the E_g term added to F will renormalize T_0' by always lowering it by an amount $2U^2\mu_0^2N_a/k_BA$, indicating that hole doping assists the transition from an insulator to a metal.

III. RESISTIVE SWITCHING IN VO_2 UNDER AN ELECTRIC FIELD

We employ Eq. (5) to simulate the IMT in VO_2 under an electric field. As shown in the inset of Fig. 1(a), we consider a VO_2 slab of a length $L = 250$ nm (along the x direction)

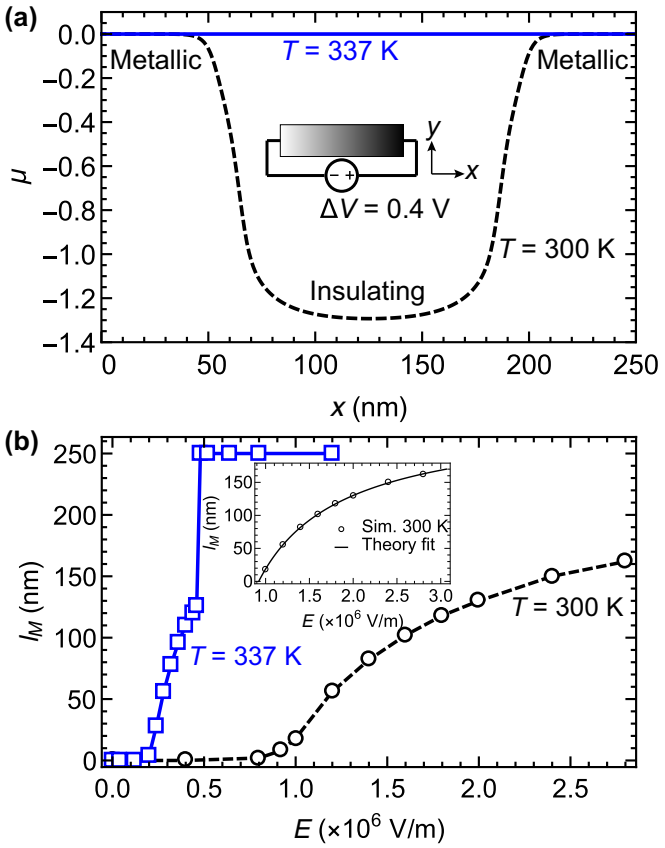

FIG. 1. (a) Spatial profiles of the spin-correlation order parameter at an applied voltage 0.4 V, outside ($T = 300$ K) and inside ($T = 337$ K) the supercooling region, respectively. The inset is a schematic of the geometry. (b) The length of the metallic region as a function of the applied electric field at the two temperatures. The lines are guide to eyes. The inset shows the theory fit of the nonzero l_M at $T = 300$ K.

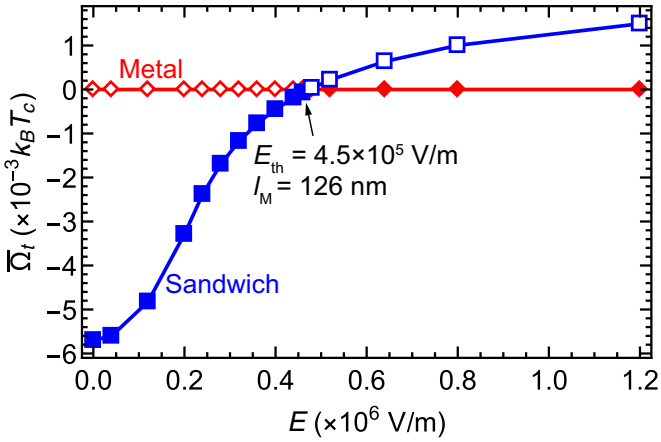

FIG. 2. Total Landau potentials of the metal-insulator-metal sandwich (blue squares) and the metal (red diamonds) as a function of the electric field at 337 K. The lines are guide to eyes. Filled and empty markers indicate stable and metastable states, respectively. The threshold E and l_M of the sandwich at the crossing point of the Landau potentials are 4.5×10^5 V/m and 126 nm, respectively, as indicated in the figure.

subject to a uniform electric field $E = \Delta V/L$ (Coulomb gauge, where ΔV is the voltage drop across the slab) in the x direction, assuming an open circuit configuration. The electric potential is $V(x) = E(x - L/2)$ as we set the $x = 0$ point at the left surface of the slab. Using the phase-field method [18], we calculate the stable states of the slab subject to an applied voltage $\Delta V = 0.4$ V, at $T = 300$ K and $T = 337$ K, which are outside and inside the supercooling region, respectively (the Landau potential yields a supercooling temperature $T_s = 309$ K). The results are shown in Fig. 1(a).

At 300 K, the two oppositely charged surfaces of the slab turn into metal that gradually grows as the electric field E increases [see Fig. 1(b)], while the middle part of the slab remains insulating, forming an insulating tunnel between the two metallic regions. The metallic regions will finally touch each other at a threshold electric field E_{th}, which essentially corresponds to the Landau-Zener tunnel breakdown [10,11]. To calculate E_{th}, we employ a theory fit to extrapolate the simulation data in Fig. 1(b), as numerical errors occur in simulations at large V due to the exponential dependence of Ω in Eq. (5) on V. Since the applied voltage creates two metal-insulator domain walls, we consider the effective domain wall repulsion induced by finite domain wall width, $F_{rep} = v \exp[-(L - l_M)/w]$ [19], with the parameters v and w to be fitted (l_M is the total length of the metallic regions). The equilibrium l_M corresponds to the minimum of the total Landau potential (including F_{rep}) with respect to l_M, which is achieved by

$$\frac{\Omega_t(x = l_M/2)|_R - \Omega_t(x = l_M/2)|_{M1}}{\mathcal{V}} + \frac{dF_{rep}}{dl_M} = 0, \quad (7)$$

where $\mathcal{V}$ is the unit cell volume of VO_2. The inset of Fig. 1(b) presents the comparison of l_M obtained from Eq. (7) and that from the simulation data, showing a good fitting yielding $v = 273$ mJ/m^2 and $w = 109$ nm. Extrapolation from the theory fit gives $E_{th} = 2.87 \times 10^7$ V/m at 300 K, which is comparable with the E_{th} measured by the experiment $\lesssim 10^8$ V/m [20] and that estimated from the Zener tunnel breakdown $\sim 4 \times 10^7$ V/m [11] for VO_2.

At 337 K, the whole slab turns into metal with a uniformly distributed zero-valued order parameter at $\Delta V = 0.4$ V. As can be seen in Fig. 1(b), the metallic regions initiated from the two surfaces first grow gradually to 126 nm as E increases, and then abruptly spread throughout the whole slab, which is in sharp contrast with the 300 K case. This behavior essentially rises from the presence of the metastable metallic phase inside the supercooling region. We plot in Fig. 2 the total Landau potentials $\bar{\Omega}_t = \int(\Omega_t + \mathcal{V}F_{gr})dx/L$ versus E of the metal-insulator-metal sandwich formed during growth of the metallic regions and the metastable metal. Here $F_{gr} = [\kappa_1(\nabla\eta)^2 + \kappa_2(\nabla\mu)^2]/2$ is the gradient energy density arising from the spatial variance of the order parameters [18], where κ_1 and κ_2 are positive constants. As can be seen in Fig. 2, at small E the total Landau potential of the metal-insulator-metal sandwich is lower than that of the metastable metal, which corresponds to the regime of the gradual growth of the metallic region. When E exceeds a small threshold value $E_{th} = 4.5 \times 10^5$ V/m, the total Landau potential of the sandwich is higher than that of the metastable metal, which stabilizes the metallic phase throughout the slab.

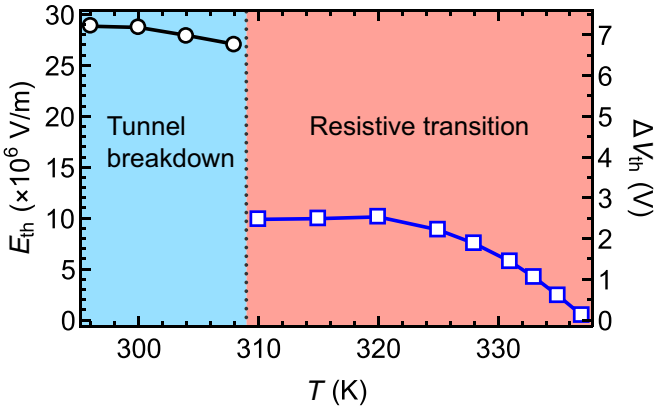

FIG. 3. Temperature-electric field phase diagram of VO_2. The threshold voltage $\Delta V_{th} = E_{th}L$ corresponding to each value of the threshold electric field is also shown on the right y axis.

The reason why the total Landau potential of the sandwich could be higher than that of the metastable metal lies in the energy loss from the two metal-insulator domain walls in the sandwich, i.e., the metal-insulator domain wall energy $F_{DW} = 2\int F_{gr}dx \sim 25$ mJ/m^2 [21]. Although the bulk Landau potential of the sandwich $(\int_0^{l_M/2} \Omega_t|_R dx + \int_{l_M/2}^{L-l_M/2} \Omega_t|_{M1} dx + \int_{L-l_M/2}^{L} \Omega_t|_R dx)/L$ is always lower than that of the metastable metal $\int_0^L \Omega_t|_R dx/L$, the total Landau potential of the sandwich (including F_{DW} and F_{rep}) and that of the metastable metal may cross for

$$2F_{DW} + F_{rep} + \left(\int_0^{l_M/2} dx\,\frac{\Omega_t|_R}{\mathcal{V}} + \int_{l_M/2}^{L-l_M/2} dx\,\frac{\Omega_t|_{M1}}{\mathcal{V}} + \int_{L-l_M/2}^{L} dx\,\frac{\Omega_t|_R}{\mathcal{V}}\right) = \int_0^L dx\,\frac{\Omega_t|_R}{\mathcal{V}},$$

or equivalently

$$\int_{l_M/2}^{L-l_M/2} dx\,\frac{\Omega_t|_R - \Omega_t|_{M1}}{\mathcal{V}} = 2F_{DW} + F_{rep}, \qquad (8)$$

signaling the genuine resistive transition during which the stable state of the slab sharply changes from the sandwich to the metal [22]. E_{th} can be calculated directly from Eq. (8) together with Eq. (7).

Figure 3 presents the threshold electric field as a function of the temperature, showing two distinct regimes separated by T_s. E_{th} drops dramatically at T_s as T increases, characterizing the similar behavior found experimentally in the VO_2 transistor [9]. For $T < T_s$, the metallic regions initiated from the two surfaces gradually grow and finally touch each other as the electric field increases, which corresponds to the smooth insulating tunnel breakdown. For $T > T_s$, the whole slab sharply turns into metal at much smaller electric fields than those in the former case due to the competition between the metal-insulator-metal sandwich and the metastable metal, which corresponds to the genuine resistive transition [22].

IV. MM PHASE IN THE VO_2-$VO_{2-\delta}$ BILAYER

As aforementioned, a MM phase was found stabilized in the VO_2-$VO_{2-\delta}$ bilayer [7]. When the VO_2 layer and the $VO_{2-\delta}$ layer are separated by an insulating TiO_2 layer, i.e., they are electronically disconnected from each other, the two layers both undergo the normal IMT as in the pristine bulk, at critical temperatures $T_{c1} \sim 290$ K and $T_{c2} \sim 280$ K, respectively [7]. However, when the $VO_{2-\delta}$ layer is epitaxially grown on the VO_2 layer, i.e., they are electronically connected with each other, the phase transition in the bilayer becomes more complicated than in the disconnected case. It was found that, while the $VO_{2-\delta}$ layer stays in the R phase between T_{c1} and T_{c2} as in the disconnected case, the MM phase is stabilized in the VO_2 layer inside this temperature interval [7].

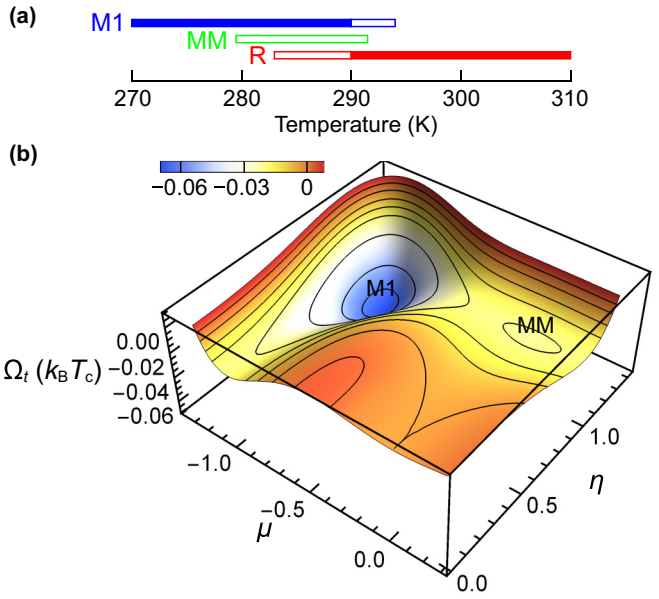

FIG. 4. (a) Stable (solid lines) and metastable (empty lines) phases of the independent hole-doped ($N_a = 5 \times 10^{-3}$ per unit cell) VO_2 thin film at various temperatures. (b) Total Landau potential landscape of the same hole-doped VO_2 thin film at 283 K, showing the stable M1 phase accompanied with the metastable MM phase.

To understand the phenomenon, we first establish a Landau potential in the same form of Eq. (1) that describes the phase transition in pristine VO_2 thin films. It is simplified such that the Landau parameters have already been renormalized by the (fixed) elastic energy (see details in Ref. [7]). The stoichiometry of the $VO_{2-\delta}$ layer is accounted for by the simultaneous -10 K shifting of T_0 and T_0' with respect to the VO_2 layer case, which simply corresponds to $T_{c2} - T_{c1} \sim -10$ K. This is simple yet sufficient to describe the phase transition in the bilayer, since in the temperature range of interest (T_{c1}–T_{c2}), the $VO_{2-\delta}$ layer remains in the R phase, and we are mainly concerned with the stable phase in the VO_2 layer. In the VO_2-$VO_{2-\delta}$ bilayer, the first principles calculation shows that the VO_2 layer is hole doped through its touching with the $VO_{2-\delta}$ layer [7]. By minimizing Eq. (6) with a typical $N_a = 5 \times 10^{-3}$ per unit cell (causing a T_0' shift ~ -10 K), we calculate the stable and metastable phases of the *independent* hole-doped VO_2 thin film at various temperatures, and the results are presented in Fig. 4(a). As can be seen, the metastable MM phase appears in the temperature interval 279–292 K, which is totally absent in the pristine case. Figure 4(b) presents the Landau potential landscape of the

same hole-doped VO_2 thin film at $T = 283$ K, showing the stable M1 phase accompanied with the metastable MM phase.

The appearance of the hole-doping-induced metastable MM phase in the VO_2 layer may lead to nontrivial phase transitions in the VO_2-$VO_{2-\delta}$ bilayer. We propose that the metastable MM phase in the VO_2 layer could further be stabilized via the interfacial interaction with the $VO_{2-\delta}$ layer and the size effect. In the temperature interval T_{c1}–T_{c2}, the $VO_{2-\delta}$ layer stays in the R phase, and a M1-R interface or a MM-R interface will form between the VO_2 and $VO_{2-\delta}$ layers depending on whether the VO_2 layer is in the M1 phase or the MM phase. The interfacial energy $2\int F_{gr}dz$ of the MM-R interface will be smaller than that of the M1-R interface, since the κ_2 term in F_{gr} almost vanishes for the MM-R interface [with $(\eta \sim 1, \mu \sim 0)$-$(\eta = 0, \mu = 0)$] while the κ_1 and κ_2 term are both finite for the M1-R interface [with $(\eta \sim 1, \mu \sim -1)$-$(\eta = 0, \mu = 0)$]. This may allow for a lower total Landau potential of the MM-R configuration than that of the M1-R configuration for the bilayer at small VO_2 layer thicknesses, at which the interfacial energy will dominate the total Landau potential. The critical thickness below which the MM-R configuration is stable can be expressed as

$$t_c = \frac{2\int dz\,(F_{gr}|_{\text{M1-R}} - F_{gr}|_{\text{MM-R}})}{\Omega_t|_{\text{MM}} - \Omega_t|_{\text{M1}}},$$

where z is the coordinate along the direction of the layer thickness.

To demonstrate this, we set up a VO_2-$VO_{2-\delta}$ bilayer geometry and employ the phase-field method [18] to calculate the total Landau potentials $\bar{\Omega}_t = \int(\Omega_t + \mathcal{V}F_{gr})dz/(t + t_0)$ of the MM-R and M1-R configurations as a function of the VO_2 layer thickness t at 283 K (t_0 is the $VO_{2-\delta}$ layer thickness). The results are shown in Fig. 5. Indeed, our model yields a $t_c \sim 9.4$ nm, which is comparable to the metal-insulator domain wall width ~10 nm found in the phase-field simulations. When the VO_2 layer thickness is below t_c, the total Landau potential of the MM-R configuration will be lower than that of the M1-R configuration, resulting in a stable MM phase in the VO_2 layer.

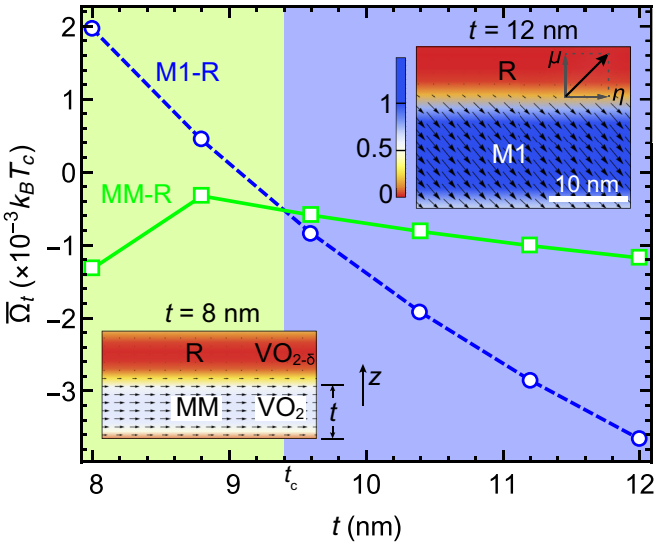

FIG. 5. Total Landau potentials (per unit cell) of the VO_2-$VO_{2-\delta}$ bilayer as a function of the VO_2 layer thickness at 283 K for the M1-R (blue circles) and MM-R (green squares) configurations. The lines are guide to eyes. The insets are the stable profiles of the order parameters for a $t < t_c$ and a $t > t_c$. The bilayer is stacked along the z direction. The arrows are the two-dimensional order parameter vector (η, μ), and the color represents its norm $\sqrt{\eta^2 + \mu^2}$.

V. CONCLUSION AND DISCUSSION

We formulated a phase-field model incorporating structural and electronic order parameters as well as free electrons and holes to describe the IMT in doped VO_2 under an electric field. The theory reveals that in the VO_2 slab under an electric field, the electric breakdown inside the supercooling region occurs through an abrupt universal IMT at threshold electric fields much smaller than those expected in the smooth Landau-Zener breakdown, in agreement with the experiment [9].

A similar phenomenon was also found in a two-orbital Hubbard model of a slab with ~20 unit cells, investigated within the dynamical mean-field theory [22]. Unlike in the microscale slab that the abrupt IMT occurs without any precursor on the insulating side [22], in our mesoscale slab ($L = 250$ nm) the metal-insulator-metal sandwich does form as a precursor before the genuine resistive transition. This difference essentially results from the different ratio of the domain wall energy over the total energy in the two scales. In the microscale slab, the domain wall energy dominates the total energy once the domain wall forms, and thus the metal-insulator-metal sandwich at its onset will have a higher total energy than the homogeneous metal. Consequently, the electric field will directly change the ground state of the slab from the homogeneous insulator to the homogeneous metal without any precursor [22]. However, in the mesoscale slab, the domain wall energy is not able to boost the total energy of the sandwich to exceed that of the homogeneous metal, until the insulating region shrinks by the electric field to a threshold length L_h [see Fig. 2, in which $L_h = (250 - 126)$ nm $= 124$ nm at $T = 337$ K]. Hence, when the slab length L is longer than L_h, the ground state of the slab does not directly change from the homogeneous insulator to the homogeneous metal by the electric field, but instead breaks from the homogeneous insulator to the inhomogeneous metal-insulator-metal sandwich before the genuine resistive transition.

When $L > L_h$, the threshold electric field E_{th} is scale independent, which can be seen through solving Eqs. (7) and (8). This qualifies the electric field as a well-defined quantity to characterize the phase diagram for $L > L_h$. We note that for $L < L_h$, however, E_{th} is *scale dependent*. In this case, the total Landau potentials of the insulator and the metal cross for $\int_0^L dx\,(\Omega_t|_R - \Omega_t|_{M1}) = 0$, giving the relation that E_{th} satisfies:

$$\frac{2k_BT_c}{eE_{th}L}\sinh\left(\frac{eE_{th}L}{2k_BT_c}\right) - 1 = \frac{F|_R - F|_{M1}}{\sqrt{N_cN_v}(E_g|_{M1} - E_g|_R)}.$$

It can be seen clearly that $E_{th} \propto L^{-1}$, and that the scale-independent quantity is the threshold voltage $\Delta V_{th} = E_{th}L$. Therefore, the well-defined quantity to characterize the phase diagram for $L < L_h$ is the voltage ΔV instead of the electric field. For this reason, we also show ΔV_{th} corresponding to each value of E_{th} in the phase diagram in Fig. 3.

It is clear that these qualitative behaviors found above by thermodynamic analysis are general for any field-driven first-order IMT.

In this work, we simplified the problem by only considering a uniform electric field or assuming the charge-neutrality approximation [22–24]. This allowed us to obtain some analytical results and interpret the essential physics more clearly. In the most precise calculation, the total electric field should be calculated self-consistently by solving the Poisson equation [25,26]. The applied electric field will be partially screened by the self-field of charged carriers. From the permittivity and carrier density yielded from capacitance measurements [27], the Debye screening length in VO_2 is estimated to be 1×10^1 to 2×10^2 nm, which may be comparable to $L/2$ and the threshold $l_M/2$. Therefore, the approximation of ignoring the self-field of carriers or charge neutrality is reasonable. Particularly if the thickness of the VO_2 film is of the order of 10 nm, as in some experiments [9,20], the screening effect along the thickness direction will be even less important, and the simplification will be valid for these experimental setups. The screening effect will make the calculated threshold electric fields higher than those calculated without it (thus approaching the experimental value), yet it shall not alter the essential physics about the resistive transition.

Employing the phase-field model, we also found that a metastable MM phase might appear in the hole-doped VO_2, which could be stabilized in the VO_2-$VO_{2-\delta}$ bilayer via the geometrical confinement and the size effect. The result may explain the presence of the stable MM phase in the VO_2-$VO_{2-\delta}$ bilayer found in the experiment [7]. Our work extends the field of the Landau theory and the phase-field method to strongly correlated systems and may offer a powerful computational method for studying the mesoscale mechanisms of IMT.

ACKNOWLEDGMENTS

This work was funded by the Penn State MRSEC, Center for Nanoscale Science, under Award No. NSF DMR-1420620.

[1] J. H. Park, J. M. Coy, T. S. Kasirga, C. Huang, Z. Fei, S. Hunter, and D. H. Cobden, Measurement of a solid-state triple point at the metal-insulator transition in VO_2, Nature (London) **500**, 431 (2013).

[2] S. Biermann, A. Poteryaev, A. I. Lichtenstein, and A. Georges, Dynamical Singlets and Correlation-Assisted Peierls Transition in VO_2, Phys. Rev. Lett. **94**, 026404 (2005).

[3] H. Zheng and L. K. Wagner, Computation of the Correlated Metal-Insulator Transition in Vanadium Dioxide from First Principles, Phys. Rev. Lett. **114**, 176401 (2015).

[4] W. H. Brito, M. C. O. Aguiar, K. Haule, and G. Kotliar, Metal-Insulator Transition in VO_2: A DFT + DMFT Perspective, Phys. Rev. Lett. **117**, 056402 (2016).

[5] Z. Tao, T.-R. T. Han, S. D. Mahanti, P. M. Duxbury, F. Yuan, C.-Y. Ruan, K. Wang, and J. Wu, Decoupling of Structural and Electronic Phase Transitions in VO_2, Phys. Rev. Lett. **109**, 166406 (2012).

[6] M. K. Liu, M. Wagner, E. Abreu, S. Kittiwatanakul, A. McLeod, Z. Fei, M. Goldflam, S. Dai, M. M. Fogler, J. Lu *et al.*, Anisotropic Electronic State via Spontaneous Phase Separation in Strained Vanadium Dioxide Films, Phys. Rev. Lett. **111**, 096602 (2013).

[7] D. Lee, B. Chung, Y. Shi, G.-Y. Kim, N. Campbell, F. Xue, K. Song, S.-Y. Choi, J. P. Podkaminer, T. H. Kim *et al.*, Isostructural Metal-Insulator Transition (unpublished).

[8] D. Wegkamp, M. Herzog, L. Xian, M. Gatti, P. Cudazzo, C. L. McGahan, R. E. Marvel, R. F. Haglund, A. Rubio, M. Wolf, and J. Stähler, Instantaneous Band Gap Collapse in Photoexcited Monoclinic VO_2 Due to Photocarrier Doping, Phys. Rev. Lett. **113**, 216401 (2014).

[9] M. Nakano, K. Shibuya, D. Okuyama, T. Hatano, S. Ono, M. Kawasaki, Y. Iwasa, and Y. Tokura, Collective bulk carrier delocalization driven by electrostatic surface charge accumulation, Nature (London) **487**, 459 (2012).

[10] L. D. Landau, Zur Theorie der Energieübertragung, Phys. Z. Sowjetunion **2**, 46 (1932).

[11] C. Zener, A theory of the electrical breakdown of solid dielectrics, Proc. R. Soc. London, Ser. A **145**, 523 (1934).

[12] Y. Wu, L. Fan, Q. Liu, S. Chen, W. Huang, F. Chen, G. Liao, C. Zou, and Z. Wu, Decoupling the lattice distortion and charge doping effects on the phase transition behavior of VO_2 by titanium (Ti^{4+}) doping, Sci. Rep. **5**, 9328 (2015).

[13] Y. Shi, F. Xue, and L.-Q. Chen, Ginzburg-Landau theory of metal-insulator transition in VO_2: The electronic degrees of freedom, Europhys. Lett. **120**, 46003 (2017).

[14] L. D. Landau and E. M. Lifshitz, *Statistical Physics*, Course of Theoretical Physics Vol. 5 (Pergamon Press, London, 1968).

[15] W. Shockley, *Electrons and Holes in Semiconductors* (D. Van Nostrand, New York, 1950).

[16] M. Rini, Z. Hao, R. W. Schoenlein, C. Giannetti, F. Parmigiani, S. Fourmaux, J. C. Kieffer, A. Fujimori, M. Onoda, S. Wall, and A. Cavalleri, Optical switching in VO_2 films by below-gap excitation, Appl. Phys. Lett. **92**, 181904 (2008).

[17] P. Debye and E. Hückel, De la theorie des electrolytes. I. Abaissement du point de congelation et phenomenes associes, Physik. Z. **24**, 185 (1923).

[18] L.-Q. Chen, Phase-field models for microstructure evolution, Annu. Rev. Mater. Res. **32**, 113 (2002).

[19] S. R. White and D. J. Scalapino, Energetics of Domain Walls in the 2D $t-J$ Model, Phys. Rev. Lett. **81**, 3227 (1998).

[20] B. Wu, A. Zimmers, H. Aubin, R. Ghosh, Y. Liu, and R. Lopez, Electric-field-driven phase transition in vanadium dioxide, Phys. Rev. B **84**, 241410 (2011).

[21] J. Wu, Q. Gu, B. S. Guiton, N. P. de Leon, L. Ouyang, and H. Park, Strain-induced self organization of metal-insulator domains in single-crystalline VO_2 nanobeams, Nano Lett. **6**, 2313 (2006).

[22] G. Mazza, A. Amaricci, M. Capone, and M. Fabrizio, Field-Driven Mott Gap Collapse and Resistive Switch in Correlated Insulators, Phys. Rev. Lett. **117**, 176401 (2016).

[23] Y.-W. Son, M. L. Cohen, and S. G. Louie, Half-metallic graphene nanoribbons, Nature (London) **444**, 347 (2006).

[24] Z. Zhang and W. Guo, Energy-gap modulation of bn ribbons by transverse electric fields: First-principles calculations, Phys. Rev. B **77**, 075403 (2008).

[25] A. N. Morozovska, E. A. Eliseev, O. V. Varenyk, Y. Kim, E. Strelcov, A. Tselev, N. V. Morozovsky, and S. V. Kalinin, Nonlinear space charge dynamics in mixed ionic-electronic conductors: Resistive switching and ferroelectric-like hysteresis of electromechanical response, J. Appl. Phys. **116**, 066808 (2014).

[26] O. V. Varenyk, M. V. Silibin, D. A. Kiselev, E. A. Eliseev, S. V. Kalinin, and A. N. Morozovska, Self-consistent modelling of electrochemical strain microscopy in mixed ionic-electronic conductors: Nonlinear and dynamic regimes, J. Appl. Phys. **118**, 072015 (2015).

[27] Z. Yang, C. Ko, V. Balakrishnan, G. Gopalakrishnan, and S. Ramanathan, Dielectric and carrier transport properties of vanadium dioxide thin films across the phase transition utilizing gated capacitor devices, Phys. Rev. B **82**, 205101 (2010).